ISSN: 2230-9926

Available online at http://www.journalijdr.com

IJDR

International Journal of Development Research
Vol. 16, Issue, 09, pp.71040-71049, September, 2026
https://doi.org/10.37118/ijdr.31181.09.2026



RESEARCH ARTICLE OPEN ACCESS

COMBINED EFFECTS OF TEMPERATURE, IRRADIATION FLUX, AND MODULATION FREQUENCY ON THE MINORITY CARRIER DENSITY DISTRIBUTION IN THE BASE OF AN IRRADIATED BIFACIAL SILICON SOLAR CELL ($N^+/P/P^+$)

Abdoulaye GUEYE[1,2], Sega GUEYE[1, 3], Gilbert Ndiasse DIONE[1,2], Ousmane DIASSE[1,3], Khady LOUM [1,2] and Idrissa GAYE [1,2]

[1]International Research Group in Renewable Energy (GIRER) BP. 15003, Dakar, Sénégal; [2]University Institute of Technology, University of Thiès, Sénégal; [3]Laboratory of Semiconductors and Solar Energy, Physics Department, Faculty of Science and Technology, University Cheikh Anta Diop, Dakar, Senegal

ARTICLE INFO

Article History:
Received 20th June, 2026
Received in revised form
25th July, 2026
Accepted 15th August, 2026
Published online 30th September, 2026

Key Words:

Bifacial silicon solar cell; Minority carrier density; Irradiation; Temperature; Modulation frequency; Carrier transport; Recombination; Continuity equation.

Corresponding author:
Abdoulaye GUEYE

ABSTRACT

This work presents a theoretical study of the combined influence of temperature, irradiation flux, damage coefficient, and modulation frequency on the distribution of the minority carrier density in the base of an irradiated silicon bifacial ($n^+/p/p^+$) solar cell. The model is based on the solution of the continuity equation under dynamic conditions with frequency-modulated polychromatic illumination, while taking into account the modifications of the transport properties induced by irradiation and temperature. The minority carrier density profiles are analyzed as a function of the base depth under different operating conditions. The results show that increasing the irradiation flux and the damage coefficient reduces the minority carrier density due to the creation of defects that enhance carrier recombination. Conversely, an increase in temperature improves carrier diffusion and leads to an increase in their density within the base. The study also highlights the effect of modulation frequency on the spatial distribution of carriers, revealing the dynamic nature of charge transport in the solar cell. These results contribute to a better understanding of the physical mechanisms governing the operation of bifacial photovoltaic solar cells subjected to harsh environments and provide a useful basis for their optimization.

Copyright©2026, Abdoulaye GUEYE et al. *This is an open access article distributed under the Creative Commons Attribution License, which permits unrestricted use, distribution, and reproduction in any medium, provided the original work is properly cited.*

Citation: ***Abdoulaye GUEYE , Sega GUEYE, Gilbert Ndiasse DIONE, Ousmane DIASSE, Khady LOUM and Idrissa GAYE. 2026.*** "Combined Effects of Temperature, Irradiation Flux, and Modulation Frequency on the Minority Carrier Density Distribution in the Base of an Irradiated Bifacial Silicon Solar Cell ($n^+/p/p^+$).". *International Journal of Development Research*, 16, (09), 71040-71049.

INTRODUCTION

Improving the performance of photovoltaic cells has become a major challenge in meeting the growing demand for clean and sustainable energy. Among the most promising technologies, bifacial silicon solar cells stand out because of their ability to convert solar radiation received on both sides, thereby offering higher conversion efficiency than conventional solar cells (1), (2), (3), (4), (5), (6), (7), (8), (9), (10), (11), (12),(13). However, their performance remains strongly dependent on operating conditions and the environmental constraints to which they are exposed. In both terrestrial and space applications, solar cellsmay be simultaneously subjected to temperature variations, energetic particle irradiation, and frequency-modulated light excitation. These factors significantly affect the charge carrier transport properties (14), (15), (16), (17), particularly the diffusion coefficient, diffusion length, and recombination probability of minority carriers (18), (19), (20), (21), (22), (23). Therefore, understanding their combined effects is essential for accurately predicting the actual behavior of photovoltaic cells and improving their design. In this context, the present work proposes a theoretical investigation of the combined influence of temperature, irradiation flux, and modulation frequency on the distribution of minority carrier density in the base of an irradiated bifacial silicon ($n^+/p/p^+$) solar cell illuminated on the front surface by frequency-modulated polychromatic light. The model is based on solving the minority carrier continuity equation (24), (25), taking into account the effects of temperature and irradiation on the diffusion coefficient and

diffusion length. The resulting minority carrier density profiles are then analyzed to highlight the influence of each parameter, as well as their combined effects, on minority carrier transport within the base of the solar cell.

MATERIALS AND METHODS

In this study, we consider an irradiated bifacial silicon ($n^+/p/p^+$) solar cell, previously exposed to charged particle irradiation characterized by the damage coefficient (kl) and the irradiation flux (Φp) (27), (28), (29), (30). A one-dimensional model (6) is adopted, in which the solar cell is illuminated on the front surface by frequency-modulated polychromatic light (14), (30). and subjected to temperature variations (T) (17), (31)..The silicon solar cell considered is illustrated in Figure 1. It consists of a front emitter of n^+ type, equipped with metallic grid contacts, heavily doped with phosphorus atoms, and having a relatively small thickness. The emitter is followed by the space-charge region, located between the emitter and the base, where a strong built-in electric field separates the photogenerated electron–hole pairs. Next is the p-type base, which is lightly doped with trivalent acceptor atoms and has a thickness much greater than that of the emitter. Finally, the structure includes a p^+ Back Surface Field (BSF) layer (12), (32), located at the rear side of the base. This region is heavily doped with acceptor atoms and generates a rear electric field that reflects minority carriers generated near the back surface toward the emitter–base junction. The BSF is well known for enhancing minority carrier collection and reducing recombination losses at the rear surface (33), (34).

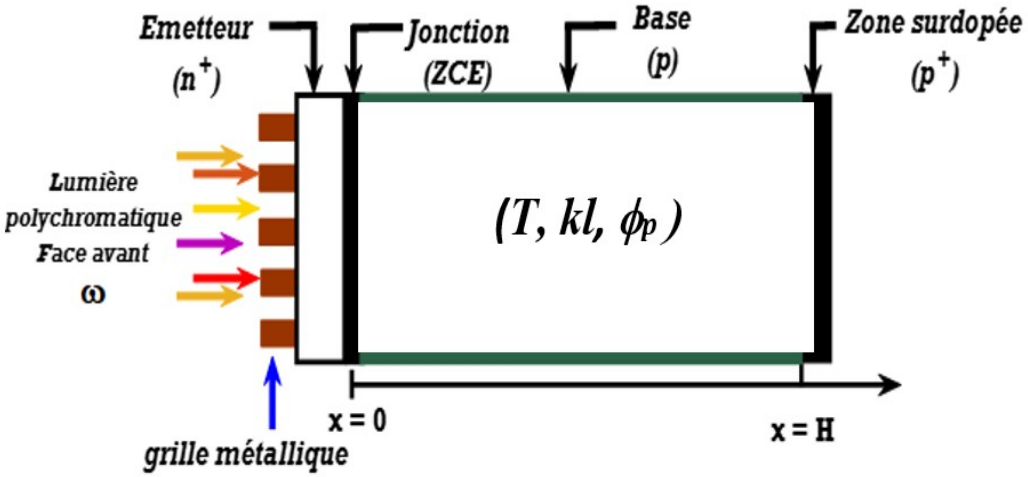


Figure 1: Structure of the bifacial silicon solar cell of type (n+/p/p+)

Continuity Equation: The continuity equation governing the excess minority carrier density, $\delta(x,t)$, in the p-type base of an irradiated silicon solar cell, characterized by the damage coefficient (kl) and irradiation flux (Φp), under frequency-modulated polychromatic illumination (ω) and temperature (T), is expressed as follows (35), (36), (37):

$$D^*(\omega, kl, \Phi p, T)\frac{\partial^2 \delta(x,t)}{\partial x^2} - \frac{\delta(x,t)}{\tau}. = -G(x,t) + \frac{\partial \delta(x,t)}{\partial t} \quad (1)$$

Where $\delta(x,t)$ denotes the excess minority carrier density in the p-type base as a function of depth (x) and time (t).

$$\delta(x,t) = \delta(x) \times e^{i\omega t} \quad (2)$$

The total carrier generation rate, (G(x,t)), as a function of depth and time, is given by (38), (39):

$$G(x,t) = g(x) \times e^{i\omega t} \quad (3)$$

Where $\delta(x)$ and g(x) represent the spatial components of the excess minority carrier density and the generation rate, respectively, while $e^{i\omega t}$ corresponds to the time-dependent harmonic component.

The spatial component of the minority carrier generation rate is expressed as

$$g(x) = n.\sum_{k=1}^{3} a_i.e^{(-b_i x)} \quad (4)$$

Where a_i and b_i are coefficients determined from tabulated solar irradiance data and depend on the wavelength-dependent absorption coefficient of silicon. These coefficients correlate the experimental illumination level with the AM1.5 standard solar spectrum.

Substituting Equations (2) and (3) into Equation (1) yields

$$\frac{\partial^2\delta(x)}{\partial x^2} - \frac{\delta(x)}{L^*(\omega,kl,\Phi p,T)^2} = -\frac{g(x)}{D^*(\omega,kl,\Phi p,T)} \quad (5)$$

c) Diffusion Coefficient $D^*(\omega, kl, \Phi p, T)$ and Diffusion Length $L^*(\omega, kl, \Phi p, T)$

The complex diffusion coefficient and the complex diffusion length of minority carriers in the p-type base of an irradiated silicon ($n^+/p/p^+$) solar cell operating under temperature variations and frequency-modulated illumination are related by the following expression (40), (41):

$$D^*(\omega, kl, \Phi p, T) \times \tau^* = L^*(\omega, kl, \Phi p, T)^2 \quad (6)$$

Where the complex carrier lifetime is

$$\tau^*(\omega) = \frac{\tau}{1+j\omega\tau} \quad (7)$$

In these expressions:

- $D^*(\omega, kl, \Phi p, T)$is the complex diffusion coefficient ;
- $\tau^*(\omega)$ is the complex minority carrier lifetime;
- $L^*(\omega, kl, \Phi p, T)$ is the complex diffusion length.

The latter is given by

$$L^*(\omega, kl, \Phi p, T) = L(kl, \Phi p, T)\sqrt{\frac{1-j\omega\tau}{1+(\omega\tau)^2}} \quad (8)$$

Minority Carrier Density: The general solution of the continuity equation describing the excess minority carrier density in the p-type base of an irradiated silicon solar cell under temperature variation and front-side frequency-modulated illumination can be written as

$$\delta_1(x, \omega, kl, \Phi p, T) = A_1 cosh\left(\frac{x}{L_\omega^*}\right) + B_1 sinh\left(\frac{x}{L_\omega^*}\right) + \sum_{i=1}^{3}\beta_i . e^{-b_i x} \quad (9)$$

With

$$\beta_i = -\frac{n a_i {L_\omega^*}^2}{D_\omega^*\left[b_i^2 {L_\omega^*}^2 - 1\right]} \quad (10)$$

$$D_\omega^* = D_\omega^*(\omega, T, kl, \Phi p) \quad (11)$$

$$L_\omega^* = L_\omega^*(\omega, T, kl, \Phi p) \quad (12)$$

The constants (A_1) and (B_1) are determined from the boundary conditions at the emitter–base junction and at the rear surface of the solar cell (42), (43), (44), (45), (46).

At the emitter–base junction (x=0)

$$\left.\frac{\partial\delta_1(x,\omega,T,kl,\Phi p)}{\partial x}\right|_{x=0} = \frac{Sf}{D_\omega^*(\omega,T,kl,\Phi p)}\delta_1(0, \omega, T, kl, \Phi p) \quad (13)$$

At the rear surface (x=H)

$$\left.\frac{\partial\delta_1(x,\omega,T,kl,\Phi p)}{\partial x}\right|_{x=H} = -\frac{Sb}{D_\omega^*(\omega,T,kl,\Phi p)}\delta_1(H, \omega, T, kl, \Phi p) \quad (14)$$

The parameters (Sf) and (Sb) denote the recombination velocities at the emitter–base junction and at the rear surface, respectively. The junction recombination velocity is expressed as the sum of two contributions: Sf = Sf0 + Sf Where (Sf0) is the intrinsic junction recombination velocity associated with losses through the shunt resistance, while (Sfj) represents the current flow imposed by an external load that determines the operating point of the solar cell (47,48).

RESULTS AND DISCUSSION

Influence of Irradiation Flux on the Minority Carrier Density

Figure 1 shows the profile of the minority carrier density as a function of the base depth x for different irradiation flux values Φp, with T= 300 K, kl = 5 cm^2/MeV , ω= $10^3 rad/s$ et $Sf = 6 \times 10^6 cm/s$

The analysis technique adopted in this study is based on the graphical representation of the minority carrier density as a function of the base depth x, as illustrated in **Figure 1**. This approach makes it possible to examine the spatial distribution of photogenerated minority carriers within the silicon base and to evaluate the influence of the irradiation flux on their transport and recombination behavior.

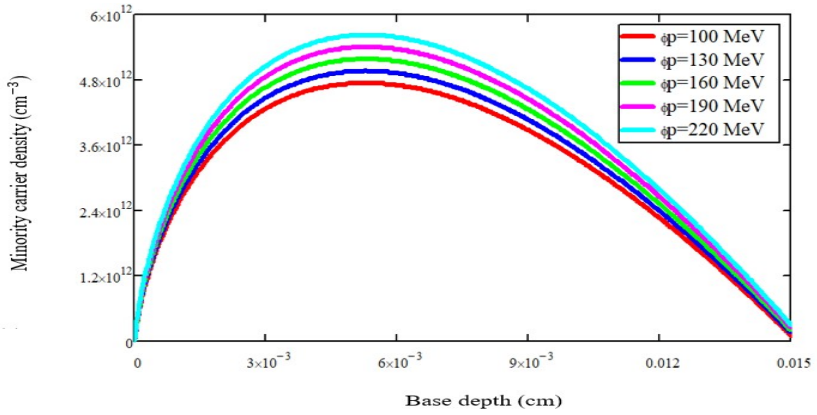


Figure 1. Minority carrier density as a function of the base depth for different irradiation flux values (T= 300 K, kl = 5 cm^2/MeV , ω= $10^3 rad/s$ et $Sf = 6 \times 10^6 cm/s$)

For base depth values x within the interval 0 cm<x<0.015 cm, the projection of the maximum point of each curve onto the vertical axis makes it possible to determine the corresponding maximum minority carrier density at that particular depth. The values of the maximum minority carrier density obtained for the different irradiation fluxes Φp are summarized in **Table 1**.

Table 1.Maximum minority carrier density as a function of the base depth for different irradiation flux values (T= 300 K, kl = 5 cm^2/MeV , ω= $10^3 rad/s$ et $Sf = 6 \times 10^6 cm/s$)

ϕp (MeV)	100	130	160	190	220
Base depth (cm)	0.0052333	0.0052333	0.0052333	0.0052333	0.0052333
Minority carrier density (cm^{-3})	$4{,}7872 \times 10^{12}$	$5{,}0000 \times 10^{12}$	$5{,}2340 \times 10^{12}$	$5{,}4468 \times 10^{12}$	$5{,}6596 \times 10^{12}$

Figure 2 shows the profile of the minority carrier density as a function of the base depth x for different irradiation flux values Φp, with T= 300 K, kl = 5 cm^2/MeV , ω= $10^3 rad/s$ et $Sf = 2 \times \frac{10^2 cm}{s}$The analysis technique adopted in this study is based on the graphical representation of the minority carrier density as a function of the base depth x, as illustrated in **Figure 1**. This approach makes it possible to examine the spatial distribution of photogenerated minority carriers within the silicon base and to evaluate the influence of the irradiation flux on their transport and recombination behavior.

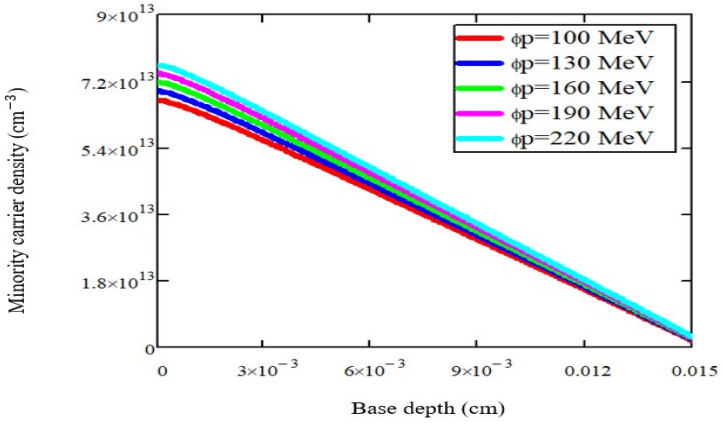


Figure 2.Minority carrier density as a function of the base depth for different irradiation flux values (T= 300 K, kl = 5 cm^2/MeV , ω= $10^3 rad/s$ et $Sf = 2 \times 10^2 cm/s$)

For base depth values x within the interval 0 cm<x<0.015 cm, the projection of the maximum point of each curve onto the vertical axis makes it possible to determine the corresponding maximum minority carrier density at that particular depth. The values of the maximum minority carrier density obtained for the different irradiation fluxes Φp are summarized in **Table 2**.

Table 2. Maximum minority carrier density as a function of the base depth for different irradiation flux values(T= 300 K, kl = 5 cm^2/MeV , ω= $10^3 rad/s$ et Sf = $2 \times 10^2 cm/s$)

ϕp (MeV)	100	130	160	190	220
$\delta(cm^{-3})$ en$x = 0cm$	$6,6781 \times 10^{13}$	$6,9230 \times 10^{13}$	$7,1624 \times 10^{13}$	$7,3966 \times 10^{13}$	$7,6256 \times 10^{13}$
$\delta(cm^{-3})$ en$x = 0,015cm$	$2,5822 \times 10^{12}$	$2,5822 \times 10^{12}$	$2,5822 \times 10^{12}$	$2,5822 \times 10^{12}$	$2,5822 \times 10^{12}$

Influence of Temperature on the Minority Carrier Density: Figure 3 shows the minority carrier density profile as a function of the base depth xxx for different temperature values T, with Φp=100MeV, kl=5 cm²/MeV, ω=10^3 rad/s, and Sf=6×10^6 cm/s. The analysis adopted in this study is based on the graphical representation of the minority carrier density as a function of the base depth xxx, as illustrated in Figure 3.

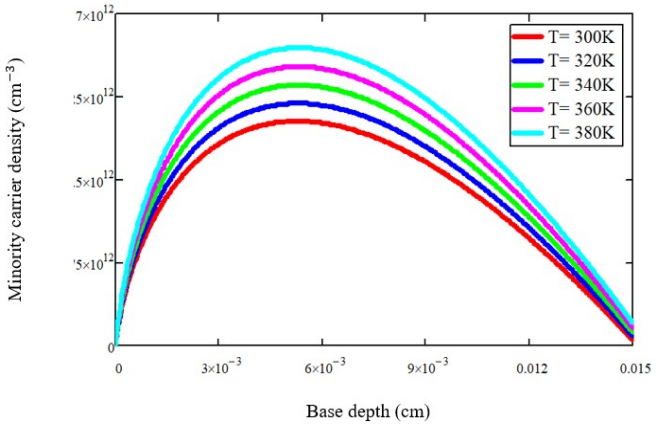


Figure 3. Minority carrier density as a function of the base depth for different temperature values (Φp=100MeV, kl=5 cm²/MeV, ω=10^3 rad/s, and Sf=6×10^6 cm/s)

For base depth values within the interval 0<x<0.015 cm, the projection of the maximum point of each curve onto the vertical axis allows the determination of the corresponding maximum minority carrier density. The values obtained for the different temperatures are summarized in **Table 3**.

Table 3.Maximum minority carrier density as a function of the base depth for different temperature values (Φp=100MeV, kl=5 cm²/MeV, ω=10^3 rad/s, and Sf=6×10^6 cm/s)

Température (K)	300	320	340	360	380
Base depth (cm)	0.0053398	0.0053398	0.0053398	0.0053398	0.0053398
Minority carrier density (cm^{-3})	4,7702 × 10^{12}	5,1653 × 10^{12}	5,5605 × 10^{12}	5,9556 × 10^{12}	6,3226 × 10^{12}

Figure 4 presents the minority carrier density profile as a function of the base depth xxx for different temperatures with Φp=100 MeV,kl=5 cm²/MeV,ω=10^3 rad/s, and Sf=2×10^2 cm/s. The adopted analysis is based on the graphical representation of the minority carrier density as a function of the base depth, as shown in **Figure 4**.

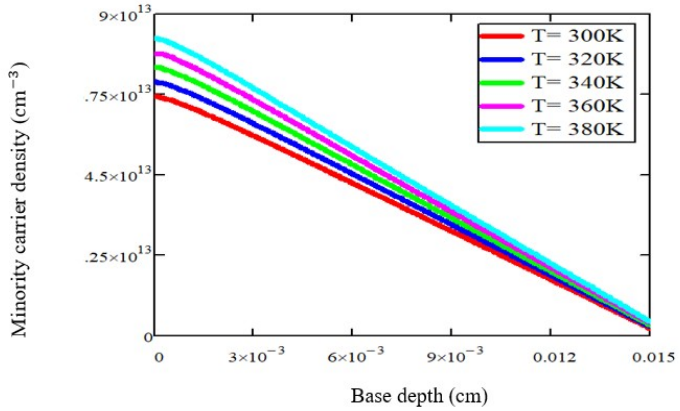


Figure 4.Minority carrier density as a function of the base depth for different temperature values (Φp=100 MeV, kl=5 cm²/MeV, ω=10^3 rad/s, and Sf=2×10^2 cm/s)

For base depths in the interval0<x<0.015 cm, the projection of the curve values at x=0 cm and x=0.015 cm onto the vertical axis provides the corresponding minority carrier densities. These values are listed in **Table 4**.

Table 4. Minority carrier density as a function of the base depth for different temperature values (Φp=100 MeV,kl=5 cm²/MeV,ω=10^3 rad/s, and Sf=2×10^2 cm/s)

Temperature (K)	300	320	340	360	380
$\delta(\mathrm{cm}^{-3})$ en$x = 0cm$	$6{,}6781 \times 10^{13}$	$7{,}0929 \times 10^{13}$	$7{,}5026 \times 10^{13}$	$7{,}9063 \times 10^{13}$	$8{,}3035 \times 10^{13}$
$\delta(\mathrm{cm}^{-3})$ en$x = 0{,}015cm$	$2{,}9779 \times 10^{12}$	$2{,}9779 \times 10^{12}$	$2{,}9779 \times 10^{12}$	$2{,}9779 \times 10^{12}$	$2{,}9779 \times 10^{12}$

Influence of the Damage Coefficient on the Minority Carrier Density: Figure 5 illustrates the minority carrier density profile as a function of the base depth xxx for different values of the damage coefficient kl, with Φp=100 MeV, T=300 K, ω=10^3 rad/s, and Sf=6×10^6 cm/s. The analysis is based on the graphical representation of the minority carrier density versus the base depth, as shown in Figure 5.

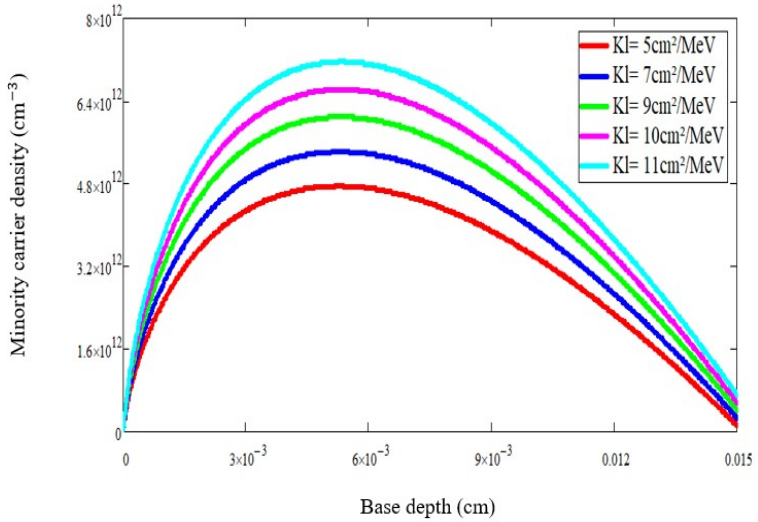


Figure 5. Minority carrier density as a function of the base depth for different values of the damage coefficient (Φp=100 MeV, T=300 K, ω=10^3 rad/s, and Sf=6×10^6 cm/s).

For 0<x<0.015 cm, the projection of the maximum point of each curve onto the vertical axis provides the corresponding maximum minority carrier density. The results are summarized in Table 5.

Table 5. Maximum minority carrier density as a function of the base depth for different values of the damage coefficient (Φp=100 MeV, T=300 K, ω=10^3 rad/s, and Sf=6×10^6 cm/s)

Kl(cm²/MeV)	5	7	9	10	11
Base depth (cm)	0.0051952	0.0051952	0.0051952	0.0051952	0.0051952
Minority carrier density (cm^{-3})	$4{,}8227 \times 10^{12}$	$5{,}5035 \times 10^{12}$	$6{,}1277 \times 10^{12}$	$6{,}6383 \times 10^{12}$	$7{,}1773 \times 10^{12}$

Figure 6 shows the minority carrier density profile as a function of the base depth for different values of the damage coefficient with Φp=100 MeV,T=300 K, ω=10^3 rad/s, and Sf=2×10^2 cm/s.

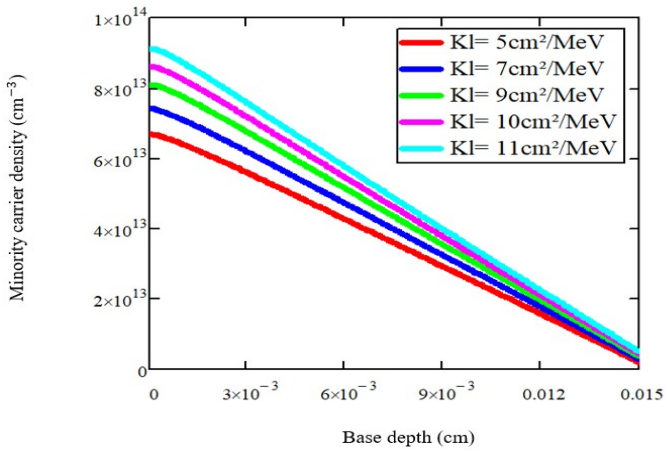


Figure 6. Minority carrier density as a function of the base depth for different values of the damage coefficient (Φp=100 MeV, T=300 K, ω=10^3 rad/s, and Sf=2×10^2 cm/s.)

For base depths between 0 and 0.015 cm, the minority carrier densities corresponding to x=0 cm and x=0.015 cm are obtained by projection onto the vertical axis. The corresponding values are presented in **Table 6**.

Table 6. Minority carrier density as a function of the base depth for different values of the damage coefficient (Φp=100 MeV, T=300 K, ω=10^3 rad/s, and Sf=2×10^2 cm/s.)

Kl(cm²/MeV)	5	7	9	10	11
Profondeur de base (cm)	0.0051952	0.0051952	0.0051952	0.0051952	0.0051952
Densité des porteurs de charge (cm^{-3})	$4{,}8227 \times 10^{12}$	$5{,}5035 \times 10^{12}$	$6{,}1277 \times 10^{12}$	$6{,}6383 \times 10^{12}$	$7{,}1773 \times 10^{12}$

Influence of the Modulation Frequency on the Minority Carrier Density: Figure 7 presents the minority carrier density profile as a function of the base depth for different modulation frequencies, with Φp=100 MeV, kl=5 cm²/MeV, T=300 K, and Sf=6×10^6 cm/s.

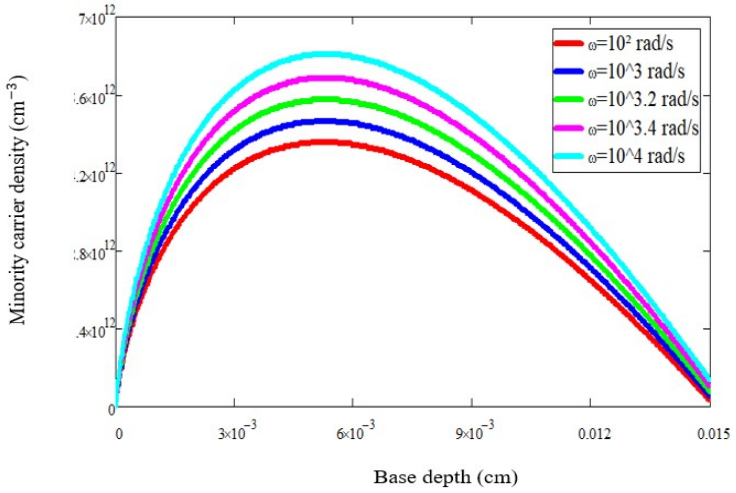


Figure 7. Minority carrier density as a function of the base depth for different modulation frequencies (Φp=100 MeV, kl=5 cm²/MeV, T=300 K, and Sf=6×10^6 cm/s)

For 0<x<0.015 cm, the projection of the maximum point of each curve onto the vertical axis gives the corresponding maximum minority carrier density. The results are summarized in **Table 7**.

Table 7.Maximum minority carrier density as a function of the base depth for different modulation frequencies (Φp=100 MeV, kl=5 cm²/MeV, T=300 K, and Sf=6×10^6 cm/s)

ω(rad/s)	10^2	10^3	$10^{3.2}$	$10^{3.4}$	10^4
Profondeur de base (cm)	0.0052244	0.0052244	0.0052244	0.0052244	0.0052244
Densité des porteurs de charge (cm^{-3})	$4{,}7935 \times 10^{12}$	$5{,}1993 \times 10^{12}$	$5{,}5543 \times 10^{12}$	$5{,}9348 \times 10^{12}$	$6{,}3406 \times 10^{12}$

Figure 8 illustrates the minority carrier density profile as a function of the base depth for different modulation frequencies with Φp =100 MeV, kl=5 cm²/MeV, T=300 K, and Sf=2×10^2 cm/s.

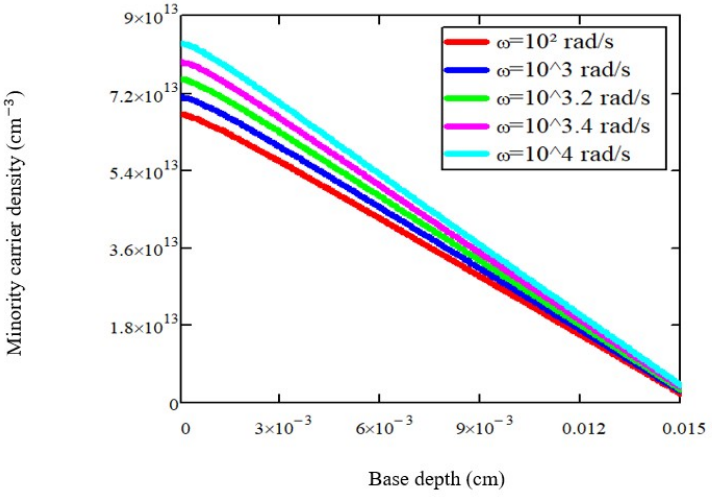


Figure 8. Minority carrier density as a function of the base depth for different modulation frequencies (Φp=100 MeV, kl=5 cm²/MeV, T=300 K, and Sf=2×10^2 cm/s).

For base depths within the interval 0<x<0.015 cm, the minority carrier densities corresponding to x=0 cm and x=0.015 cm are obtained by projection onto the vertical axis. These values are presented in **Table 8**.

Table 8.Minority carrier density as a function of the base depth for different modulation frequencies (Φp=100 MeV, kl=5 cm²/MeV, T=300 K, and Sf=2×10² cm/s)

ω(rad/s)	10^2	10^3	$10^{3.2}$	$10^{3.4}$	10^4
$\delta(cm^{-3})$ en $x = 0cm$	$6{,}7137 \times 10^{13}$	$7{,}1129 \times 10^{13}$	$7{,}4758 \times 10^{13}$	$8{,}0202 \times 10^{13}$	$8{,}3468 \times 10^{13}$
$\delta(cm^{-3})$ en $x = 0{,}015cm$	$2{,}1774 \times 10^{12}$	$2{,}1774 \times 10^{12}$	$2{,}1774 \times 10^{12}$	$2{,}1774 \times 10^{12}$	$2{,}1774 \times 10^{12}$

Combined Influence of Irradiation, Temperature, and Modulation Frequency on the Minority Carrier Density

The results demonstrate that irradiation, temperature, and modulation frequency jointly influence the distribution of the minority carrier density within the base of the bifacial silicon solar cell. Irradiation generates crystal defects that enhance carrier recombination and reduce the minority carrier density. An increase in temperature modifies the carrier transport and recombination mechanisms, whereas higher modulation frequencies shorten the time available for carrier diffusion through the base. These physical processes occur simultaneously and collectively affect carrier transport. Overall, their combined action disturbs the transport of minority carriers and leads to a reduction in their density when irradiation-induced defects and high-frequency effects become dominant. Consequently, the collected photocurrent may decrease, resulting in a degradation of the solar cell performance, particularly in the presence of internal parasitic resistances and shunt resistance.

CONCLUSION

This study investigated the distribution of the minority carrier density in the base of an irradiated bifacial silicon (n+/p/p+) solar cell by considering the combined effects of temperature, irradiation flux, damage coefficient, and modulation frequency. By solving the continuity equation, minority carrier density profiles were established and analyzed under various operating conditions. The results indicate that increasing the irradiation flux and the damage coefficient leads to a reduction in the minority carrier density due to the generation of crystal defects that enhance carrier recombination. Conversely, increasing the temperature promotes carrier diffusion and increases the minority carrier density within the base of the solar cell. The study also highlights the influence of modulation frequency on the spatial distribution of minority carriers, emphasizing the dynamic nature of carrier transport under modulated illumination. These findings provide a deeper understanding of the physical mechanisms governing the behavior of bifacial silicon solar cells operating under varying irradiation and temperature conditions. They also provide a valuable basis for optimizing the operating conditions and design parameters of photovoltaic devices intended for use in highly irradiated environments.

REFERENCES

1. M.A. Green, (March 1995). Silicon Solar cells advanced principles & practice Printed by Bridge printer Pty. Ltd. 29-35 Dunning Avenue, Roseberry, Center for photovoltaic Devices and systems; pp.29-35.
2. Gover, A. and Stella, P. (1974). Vertical Multijunction Solar-Cell One-Dimensional Analysis. IEEE Transactions on Electron Devices, Vol. ED-21: 6. pp.351-356, https://doi.org/10.1109/T-ED.1974.17927
3. A. A. Cuevas, A. luque, and J. M. Ruiz, A, (1980). n+/p/n+ double-sided solar cell for optimal static concentration, in Proc. 14th IEEE Ptotov. Spec. Conf., San Diego, pp.76-81.
4. Luque, A., Ruiz, J.M., Cuevas, A., Eguren, J. and Agost, M.G. (1997) Double Side Solar Cells to Improve Static Concentrator. Photovoltaic Solar Energy Conference, Luxembourg, 269-277. https://doi.org/10.1007/978-94-009-9840-7_25
5. Hüber, A., Aberle, A.G. and Hezel, R. (2001) 20% Efficient Bifacial Silicon Solar Cells. Munich 14th European Photovoltaic Solar Energy Conference, 1796-1798.
6. Wise, J.F. (1970) Vertical Junction Hardened Solar Cell. U.S. Patent 3, 690-953.
7. Cuevas, A., Sinton, R.A. and King, R.R. (1991) A Technology-Based Comparison between Two-Sided and Back-Contact Silicon Solar Cells. The 10th European Photovoltaic Solar Energy Conference, Lisbon, 8-12 April 1991, 23-26.
8. Bordin, N., Kreinin, L. and Eisenberg, N. (2001) Determination of Recombination Parameters of Bifacial Silicon Cells with a Two Layer Step-Liked Effect Distribution in the Base Region. Proc. 17th European PVSEC, Munich, 1495-1498.
9. Martin A. Green (2013). High-Efficiency Silicon Solar Cell Concepts. Chapter published 2013 in Solar Cells, Pp. 87-113 http://dx.doi.org/10.1016/b978-0-12-386964-7.00005-6
10. Nam, L.Q., Rodot, M., Ghannam, M., Cppye, J. and de Schepper, P.J. (1992) Solar Cells with 15.6% Efficiency on Multicristalline Silicone, Using Impurity Gettering, back Surface Field and Emitter Passivation. International Journal of Solar Energy, 11, 273-279. https://doi.org/10.1080/01425919208909745
11. Fossum, J.G. and Burgess, E.L. (1978) High Efficiency p+-n-n+ Back-Surface-Field Solar Cells. Applied Physics Letters, 33, 238-240.https://doi.org/10.1063/1.90311

12. E.Gaubas and J. Vanhellemont (1996). A simple Technique for the Separation of Bulk and Surface Recombination Parameters in Silicon. Journal of Applied Physics, 80, 6293-6297. https://doi.org/10.1063/1.363705M
13. Meier, D.L., Hwang, J.-M. and Campbell, R.B. (1988) The Effect of Doping Density and Injection Level on Minority Carrier Lifetime as Applied to Bifacial Dendritic Web Silicon Solar Cells. IEEE Transactions on Electron Devices, 35, 70-79. https://doi.org/10.1109/16.2417
14. Denise, K., Mamadou, L.B., Mamour, A.B., Gora, D., El Hadj, S., Oulimata, M. and Gregoire, S. (2020) AC Back Surface Recombination in n^+-p-p^+ Silicon Solar Cell: Effect of Temperature. International Journal of advanced Research (IJAR), 8, 140-151.
https://doi.org/10.21474/IJAR01/11273
15. Richard Mane, Ibrahima Ly, Mamadou Wade, IbrahimaDatta, Marcel S. Douf, YoussouTraore, Mor Ndiaye, Seni Tamba, Grégoire Sissoko (2017). Minority Carrier Diffusion Coefficient D*(B, T): Study in Temperature on a Silicon Solar Cell under Magnetic Field. Energy and Power Engineering, 9, pp.1-10 http://www.scirp.org/journal/epe
16. Seydina, D., Mor, N., Ndeye, T., Youssou, T., Mamadou, L.B., Ibrahima, D., Marcel, S.D., Oulimata, M., Amary, T. and Grégoire, S. (2019). Influence of Temperature and Frequency on Minority Carrier Diffusion Coefficient in a Silicon Solar Cell Under Magnetic Field. Energy and Power Engineering, 11, 355-361. &https://doi.org/10.4236/epe.2019.1110023
17. Ibrahima Tall, Boureima Seibou, Mohamed Abderrahim Ould El Moujtaba, Amadou Diao, Mamadou Wade, Gregoire Sissoko (2015). Diffusion Coefficient Modeling of a Silicon Solar Cell under Irradiation Effect in Frequency: Electric Equivalent Circuit. *International Journal of Engineering Trends and Technology (IJETT) – Volume 19 Number 2 – p.56-61, Jan 2015* (http://www.ijettjournal.org).
18. M. A. Ould El Moujtaba, M. Ndiaye, A. Diao, M. Thiam, I. F. Barro and G. Sissoko (2012). Theorical Study of Influence of Irradiation on a Silicon Solar Cell Under Multispectral Illumination. Research Journal of Applied Sciences Engineering and Technolgy, Vol. 23, Issue 4, pp.5068-5073, 2012.
19. I. Gaye, R. Sam, A. D. Seré, I. F. Barro, M. A. Ould El Moujtaba, R. Mané, G. Sissoko (2012). Effect of irradiation on the transient response of a silicon solar cell; International journal of emerging trends and technologies in computer science (IJETTCS) Volume 1, Issue 3, September-October 2012, ISSN 2278-6856.
20. I. Ly, M. Wade, H. Ly Diallo, M. A. O. El Moujtaba, O. H. Lemrabott, S. Mbodji, O. Diasse, A. Ndiaye, I. Gaye, F. I. Barro, A. Wereme, G. Sissoko (2011). Irradiation effect on the electrical parameters of a bifacial silicon solar cell under multispectral illumination», Proceedings of 26th European Photovoltaic Solar Energy Conference and Exhibition 1DV.4.52 (2011), pp 785-788; http://www.eupvsec-proceedings.com
21. Ndeye Madeleine Diop, Boureima Seibou, Mamadou Wade, Marcel Sitor Diouf, Ibrahima Ly, Hawa Ly Diallo, Gregoire Sissoko (2016). Theoretical Study of Vertical Parallel Junction Silicon Solar Cell Capacitance under Modulated Polychromatic Illumination: Influence of Irradiation. International Journal of Innovative Technology and Exploring Engineering (IJITEE) ISSN:2278-3075, Volume-6 Issue-3, August 2016).
22. Mouhamadou Mousliou Diallo, Seni Tamba, Boureima Seibou, Mohamed LemineOuld Cheikh, Ibrahima Diatta, El Hadji Ndiaye, Youssou Traore, Cheikh Tidiane Sarr, Gregoire Sissoko (2017). Impact of irradiation on the surface recombination velocity of a back side monochromatic illuminated bifacial silicon solar cell under frequency modulation, Journal of Scientific and Engineering Research, 2017, 4(1): 29-40
23. Ba, M.L., Diallo, H.L., Ba, H.Y., Traore, Y., Diatta, I., Diouf, M.S., Wade, M. and Sissoko, G. (2018). Irradiation Energy Effect on a Silicon Solar Cell: Maximum Power Point Determination. Journal of Modern Physics, 9, 2141-2155. https://doi.org/10.4236/jmp.2018.912135
24. G.Sissoko, C. Museruka, A. Corréa, I. Gaye and A.L.Ndiaye, Light Spectral Effect on Recombination Parameters of Silicon Solar Cell. World Renewable Energy Congress, Pergamon, Part III, pp.1487-1490.
25. Ba. M.L., Thiam, N., Thiame, M., Traore, Y., Diop, M.S., Ba, M., Sarr, C.T., Wade, M. and Sissoko, G. (2019). Base Thickness Optimization of a (n+-p-p+) Silicon Solar Cell in Static Mode under Irradiation of Charged Particles. Journal of Electromagnetic Analysis and Applications, 11, 173-185. https://doi.org/10.4236/jemaa.2019.1110012
26. Ohshima, T., T. Sumita, M. Imaizumi, S. Kawakita, K. Shimazaki, S. Kuwajima, A. Ohi, And H. Itoh (2005). Evaluation of the Electrical Characteristics of III-V Compounds Solar Cells Irradiated with Protons at Low Temperatures. Proceedings of the 31st IEEE Photovoltaic Specialists Conference: 806
27. Kraner, H. W., Radiation damage in silicon detectors, 2nd Pisa Meeting on Advanced Detectors, Grosetto, Italy, June 3-7 1983.
28. Goo-Hwan Shin and Kwangsun Ryu and Hyung-Myung Kim and Kyung-wook Min (2008). Radiation effect test for single-crystalline and polycrystalline silicon solar cells. Journal of the Korean Physical Society. Vol. 52, Pp. 843-847. https://api.semanticscholar.org/CorpusID:120466620
29. Ly Diallo, H., Wade, M., Ly, I., NDiaye, M., Dieng, B., Lemrabott, O.H., Maïga, A.S. and Sissoko. G. (2012). 1D Modeling of a Bifacial Silicon Solar Cell under Frequency Modulation, Monochromatic Illumination: Determination of the Equivalent Electrical Circuit Related to the Surface Recombination Velocity. Research Journal of Applied Sciences, Engineering and Technology, 4, 1672-1676. http://www.maxwell.org.
30. Konstantinos Misiakos and Dimitris Tsamakis, Electron and Hole Mobilities in Lightly Doped Silicon. Appl. Phys. Lett.1994, 64(15),2007-2009. https://doi.org/10.1063/1.111721
31. O. Diasse, R. S. Sam, H. L. Diallo, M. Ndiaye, N. Thiam, S. Mbodji and G. Sissoko, Solar cell's classification by the determination of the specific values of the back surface recombination velocities in open circuit and short-circuit operating conditions. International Journal of Emerging Trends & Technology in Computer Science (IJETTCS), 2012, 2278/6856:18-23)

32.H.L.Diallo, A. Seïdou. Maiga, A.Wereme and G.Sissoko, New Approach of Both Junction and Back Surface Recombination Velocities in a 3D Modelling Study of a Polycrystalline Silicon Solar Cell. The European Physical Journal Applied Physics,2008, 42, 203-211. http://dx.doi.org/10.1051/epjap:2008085

33.Masse Samba Diop , Hamet Yoro Ba , Ndeye Thiam , Ibrahima Diatta , Youssou Traore , Mamadou Lamine Ba , El Hadji Sow , Oulymata Mballo , Grégoire Sissoko, Surface Recombination Concept as Applied to Determinate Silicon Solar Cell Base Optimum Thickness with Doping Level EffectWorld Journal of Condensed Matter Physics, 2019, 9, 102-111 https://www.scirp.org/journal/wjcmp

34.G.Sissoko, C. Museruka, A. Corréa, I. Gaye and A.L.Ndiaye, Light Spectral Effect on Recombination Parameters of Silicon Solar Cell. World Renewable Energy Congress, Pergamon, Part III, pp.1487-1490.

35.Dieng, A., Zerbo, I., Wade, M., Maiga, A.S. and Sissoko, G. (2011) Three-Dimensional Study of a Polycrystalline Silicon Solar Cell: The Influence of the Applied Magnetic Field on the Electrical Parameters. Semiconductor Science and Technology, 26, Article ID: 095023.https://doi.org/10.1088/0268-1242/26/9/095023.

36.Thiam. N, Diao. A, Ndiaye. M, Dieng. A, Thiam.A, Sarr. M, Maiga. A.S and Sissoko G. (2012). Electric Equivalent Models of Intrinsic Recombination Velocities of a Bifacial Silicon Solar Cell under Frequency Modulation and Magnetic Field Effect. Research Journal of Applied Sciences, Engineering and Technology, 4, 4646-4655.

37.Furlan, J. and Amon, S. (1985). Approximation of the Carrier Generation Rate in Illuminated Silicon. Solid-State Electronics, 28, 1241-1243. https://doi.org/10.1016/0038-1101(85)90048-6.

38.M. A. Green, K. Emery, D. L. King, Y. Hishikawa, and W. Warta, (2006). 'Solar Cell Efficiency Tables (version 28)', Progress in Photovoltaics: Research and Applications, vol. 14; pp. 455–461.

39. Teya, M. , Sow, O. , Loum, K. , Diatta, I. , Diop, G. , Traore, Y. , Wade, M. and Sissoko, G. (2023) Determination of the Base Optimum Thickness of Back Illuminated ($n^+/p/p^+$) Bifacial Silicon Solar Cell, by Help of Diffusion Coefficient at Resonance Frequency. *Journal of Electromagnetic Analysis and Applications*, **15**, 13-24. doi: 10.4236/jemaa.2023.152002.

40. Diop, G. , Sow, O. , Thiame, M. , Mane, R. , Diatta, I. , Loum, K. , Gueye, S. , Wade, M. and Sissoko, G. (2022). Diffusion Coefficient at Double Resonances in Frequency and Temperature, Applied to ($n^+/p/p^+$) Silicon Solar Cell Base Thickness Optimization under Long Wavelength Illumination. *Journal of Electromagnetic Analysis and Applications*, **14**, 89-103. doi: 10.4236/jemaa.2022.148008.

41.O. Diasse, R. S. Sam, H. L. Diallo, M. Ndiaye, N. Thiam, S. Mbodji and G. Sissoko, Solar cell's classification by the determination of the specific values of the back surface recombination velocities in open circuit and short-circuit operating conditions. International Journal of Emerging Trends & Technology in Computer Science (IJETTCS), 2012, *2278/6856*:18-23)

42.O.Diasse. A. Diao, I. Ly, M.S. Diouf. I. Diatta. R.Mane. Y. Traore and G.Sissoko, Back Surface Recombination Velocity Modeling in White Biased Silicon Solar Cell under Steady State. Journal of Modern Physics, 2018, 9, 189-201.

43.I. Ly, M. Ndiaye, M. Wade, N. Thiam, S. Gueye and G. Sissoko, Concept of Recombination Velocity Sfcc at the Junction of a Bifacial Silicon Solar Cell, in Steady State, Initiating the Short-Circuit Condition. Research Journal of Applied Sciences, Engineering and Technology,2013, 5, 203-208. https://doi.org/10.19026/rjaset.5.5105

44.Y. Traore, N. Thiam, M. Thiame, M. L. Ba, M. S. Diouf et G. Sissoko, AC Recombination Velocity in the Back Surface of a Lamella Silicon Solar Cell under Temperature.*Journal of Modern Physics,*2019,10, 1235-1246. https://doi.org/10.4236/jmp.2019.1010082

45.M. Gueye, H. L. Diallo, A. Kosso, M. Moustapha, Y. Traore, I. Diatta et G. Sissoko, Ac Recombination Velocity in a Lamella Silicon Solar Cell. World Journal of Condensed Matter Physics, 2018,8, 185-196.

46.Ndiaye, E.H., Sahin, G, Dieng, M., Thiam, A, Diallo, H.L., Ndiaye, M. and Sissoko, G. (2015) Study of the Intrinsic Recombination Velocity at the Junction of Silicon Solar under Frequency Modulation and Irradiation. Journal of Applied Mathematics and Physics, 3, 1522-1535. https://doi.org/10.4236/jamp.2015.311177

****